Journal of Alloys and Compounds 506 (2010) 285–292

Contents lists available at ScienceDirect

Journal of Alloys and Compounds

journal homepage: www.elsevier.com/locate/jallcom

Electrical conductivity and oxygen sensing behavior of $SrSn_{1-x}Fe_xO_{3-\delta}$ ($x = 0$–0.2)

Sunasira Misra[a], K.I. Gnanasekar[a,*], R.V. Subba Rao[b], V. Jayaraman[a], T. Gnanasekaran[a]

[a] Liquid Metals and Structural Chemistry Division, Indira Gandhi Centre for Atomic Research, Kalpakkam 603 102, India
[b] Corrosion Science and Technology Division, Indira Gandhi Centre for Atomic Research, Kalpakkam 603 102, India

ARTICLE INFO

Article history:
Received 28 April 2010
Received in revised form 22 June 2010
Accepted 1 July 2010
Available online 7 July 2010

Keywords:
Oxides
Electrical conductivity
X-ray photoemission spectroscopy
Mossbauer effect

ABSTRACT

$SrSn_{1-x}Fe_xO_{3-\delta}$ ($x = 0$, 0.05, 0.1, 0.15 and 0.2) exhibiting cubic structure (S.G.: P23) have been prepared by solid state route. Electrical conductivity increases with Fe concentration. Activation energy E_a values deduced from the Arrhenius plots of the respective compositions are in the range of 0.4–0.45 eV which imply that the mechanism of electrical conduction is same for all the compositions except for $x = 0$. X-ray photoelectron spectroscopy studies reveal that the valence states of Sr, Sn and oxygen are respectively +2, +4 and −2. Mossbauer spectroscopy studies reveal that Fe-ions in tetravalent, trivalent and divalent states with their relative proportion remain more or less same across the compositions. The increase in conductivity is due to lower valence Fe-ions. Among these compositions, $SrSn_{0.85}Fe_{0.15}O_{3-\delta}$ exhibits significant changes in conductivity as function of oxygen partial pressure and becomes a promising composition for percentage level oxygen sensor as revealed by the sensor studies.

1. Introduction

Materials possessing high thermal stability and offering the scope for tailoring its physical properties using dopants have become the centre of investigation in the field of chemical sensors. Strontium stannates have been reported to be promising sensor materials for oxygen ($T > 873$ K) [1,2]. They exhibit significant conductivity only above 873 K and therefore the sensors made of them have to be operated at high temperatures. In order to bring down the operating temperature of the existing materials, substitutions at different lattice sites become the logical approach for investigation. $SrSnO_3$, a perovskite (ABO_3) with a band gap of 1.7 eV is chosen for its favorable chemically stability and its tolerance towards large-scale substitution either in A-site or B-site with the retention of the structure [3,4–6]. Generally A-site (12 coordinated alkaline earth metal ion) dopants contribute to ionic conduction and B-site (6 coordinated transition metal ion) dopants contribute to electronic conduction [7]. It has been found that the partial substitution of tetravalent tin by alio-valent cations improves the electrical conductivity [8]. Electrical conductivity of iron substituted $SrSn_{1-x}Fe_xO_3$ have been investigated as a function of oxygen partial pressure and temperature. Iron rich $SrSn_{1-x}Fe_xO_3$ ($x > 0.7$) has been shown to be an electronic conductor over a wide range of oxygen partial pressure above 873 K and suggested to be a candidate material for cathodes in SOFCs [1,5]. On the other hand, the iron deficient $SrSn_{1-x}Fe_xO_3$ ($x < 0.3$) is a mixed conduction system (oxide ion and electronic) and therefore it is expected to be a promising system for gas sensor applications [5,6]. This paper reports the results of our investigation on preparation, structural and electrical conductivity characterization, X-ray photoelectron spectroscopy (XPS), Mossbauer studies and the sensor characterization of $SrSn_{1-x}Fe_xO_{3-\delta}$ ($x \leq 0.2$) for different percentage levels of oxygen. The objective of this work is to find out the highly sensitive composition which exhibits large changes in conductivity in the oxygen partial pressure range of 10–21% within the family of $SrSn_{1-x}Fe_xO_{3-\delta}$.

2. Experimental

Nominal compositions of $SrSn_{1-x}Fe_xO_{3-\delta}$ ($0 < x < 0.2$) were prepared by solid state route by taking appropriate amounts of $SrCO_3$ (99.9% purity, M/s Aldrich, USA), SnO_2 (99% purity, E. Merck, Germany) and Fe_2O_3 (99.9% purity, M/s Aldrich, USA). The mixtures were ground using Agate mortar and pestle with a few drops of acetone (AR grade M/s E. Merck, India). The mixed powders were uniaxially pressed into pellets at 3 MPa and calcined in air for 10 h at 1173 K for decarbonation. The pellets were reground, made again in the form of pellets and heated to 1573 K at a rate of 10 K/min from room temperature. The samples were sintered at this temperature for 24 h and then cooled to room temperature. This process was repeated twice with intermittent grinding of the samples in order to get homogenous products. The XRD patterns of the samples were recorded using X-ray powder diffractometer (model D-500 of M/s Siemens, Germany) with Cu Kα radiation ($\lambda = 1.5418$ Å). Crystallographic phase analysis of the individual compositions was checked. Pellets (8 mm diameter and approximately 2 mm thickness) from each composition was mounted between two spring-loaded platinum foils of identical dimensions and placed inside a quartz chamber which in turn was heated by a furnace. The temperature dependence of electrical conductivity of these samples under three different oxygen partial pressures viz. 100% O_2, 21% O_2 in air and argon containing 10 (±2) ppm of O_2 (analyzed by a calibrated electrochemical oxygen sensor) was investigated in the temperature range of 383–823 K. A frequency response analyzer (Model SI 1260 of Solartron, M/s Schlumberger, UK) coupled with an electrochemical interface (Model 1287 of

* Corresponding author. Tel.: +91 44 27480098; fax: +91 44 27480065.
E-mail address: igsk@igcar.gov.in (K.I. Gnanasekar).

0925-8388/$ – see front matter © 2010 Elsevier B.V. All rights reserved.
doi:10.1016/j.jallcom.2010.07.005

Solartron, M/s Schlumberger, UK) in the frequency range 100 Hz to 1 MHz was used for this study under the application of 500 mV perturbation voltage to the sample. X-ray photoelectron spectra of these samples were recorded to estimate various elemental oxidation states using SPECS make (Germany) spectrophotometer with 150 mm hemispherical analyzer at band pass energy of 12 eV. Monochromatised Al Kα X-ray radiation of 1486.74 eV was used. XPS analysis were carried out in pellet specimens at room temperature under a vacuum of 7×10^{-10} mbar. The binding energy value of carbon 1s was also recorded for correction arising out of charging. In addition, Mossbauer spectroscopy was used to investigate the valence states of Fe in these samples. For these studies, powder samples were mixed with $LiCO_3$ as matrix and taken for spectral analysis. Mossbauer spectra were recorded using the spectrometer of electro-mechanical type at room temperature with 25 mCi ^{57}Co in rhodium matrix as source in constant acceleration mode (WISSEL, Germany). Velocity calibrations were carried out using standard α-Fe. Data fitting was carried out using least square fitting program (NORMOS) considering Lorentz shape function. The isomer shift values reported in this paper are with respect to α-Fe at room temperature (301 K). Oxygen sensing characteristics of the bulk porous pellet sensors were studied for various partial pressures of oxygen at different temperatures. The conductivity cell described for mounting the pellet specimen for ac-impedance technique is used for sensor studies also. Impedance spectra are recorded under equilibrium conditions when the frequency is swept from 100 Hz to 1 MHz. This requires about 2 min and hence it is not suitable for measuring the transient changes in conductivity during sensing. Therefore, the two-probe dc technique is adopted for measuring the transient changes in conductivity. For maintaining different partial pressures of oxygen in argon, mass flow controllers (Model No. DFC 2600, M/s AALBORG Instruments, USA) were used. Different quantities of oxygen gas were mixed with argon while the total flow rate was maintained at 20 ml/min. During gas sensing, data were continuously collected using data acquisition system (Model No. 34970A, M/s Agilent, Malaysia). The percentage response for a change in partial pressure of oxygen was calculated as follows:

$$\% \text{ Response} = [(R - R_o)/R] \times 100$$

where R_o is the resistance of the sensor in air and R is the resistance of the sensor in the ambient of different partial pressures of oxygen.

3. Results and discussion

XRD patterns of $SrSn_{1-x}Fe_xO_{3-\delta}$ ($0 < x < 0.2$) samples are shown in Fig. 1. All the reflections are indexed in terms of cubic pattern [S.G.: P23 (195), JCPDS # 74-1298] of the perovskite structure. No other reflections corresponding to any impurity are observed indicating that all the samples are phase pure. However, Beurmann and co-workers who investigated the compatibility of $SrSnO_3$–$SrFeO_3$ systems have reported that $SrSn_{1-x}Fe_xO_{3-\delta}$ ($0 < x < 0.2$) stabilized in orthorhombic structure [S.G.: Pbnm (JCPDS # 77-1798)] as against the cubic phase observed by us although the same synthesis conditions such as heating schedules, temperature, etc., are followed [9]. $SrSnO_3$ is an ideal perovskite having Sr-ions in 12-fold coordination and Sn-ions in 6-fold coordination as shown in Fig. 2. In $SrSn_{1-x}Fe_xO_{3-\delta}$ cubic perovskite unit cell, Fe is expected to occupy the Sn site in this structure as the ionic radius of Sr^{2+} (1.44 å) is too large to accommodate iron while the ionic size of Sn^{4+} is close to that of Fe ions (ionic radius of Fe^{4+}, Fe^{3+}, Fe^{2+} in 6-fold coordination are 0.585, 0.645 and 0.78 å respectively and the ionic radius of Sn^{4+} is 0.69 å) [10]. Lattice cell parameters were calculated for different levels of iron substitution and the plot of cell volume as a function of concentration of Fe is shown in Fig. 3. As anticipated, the lattice parameter and the cell volume was found to decrease from 4.0294(±0.0003) å to 4.0129(±0.0003) å for iron concentration $x = 0$–0.2 respectively which agrees well with the reported values [1,9,11]. Cell volume also decreases systematically with increase in Fe concentration (Fig. 3).

Electrical conductivity studies on all the samples were carried out in the temperature range of 473–723 K under different partial pressures of oxygen in air typically (10–30%) with and without the presence of moisture. Results of our investigation of temperature dependence of electrical conductivities of $SrSn_{1-x}Fe_xO_{3-\delta}$ ($x = 0$–0.2) in air are shown in the form of Arrhenius plot in Fig. 4. It is clear that electrical conductivity values are systematically increasing as the Fe concentration is increased. The slopes of the Arrhenius plots are nearly same for all the compositions

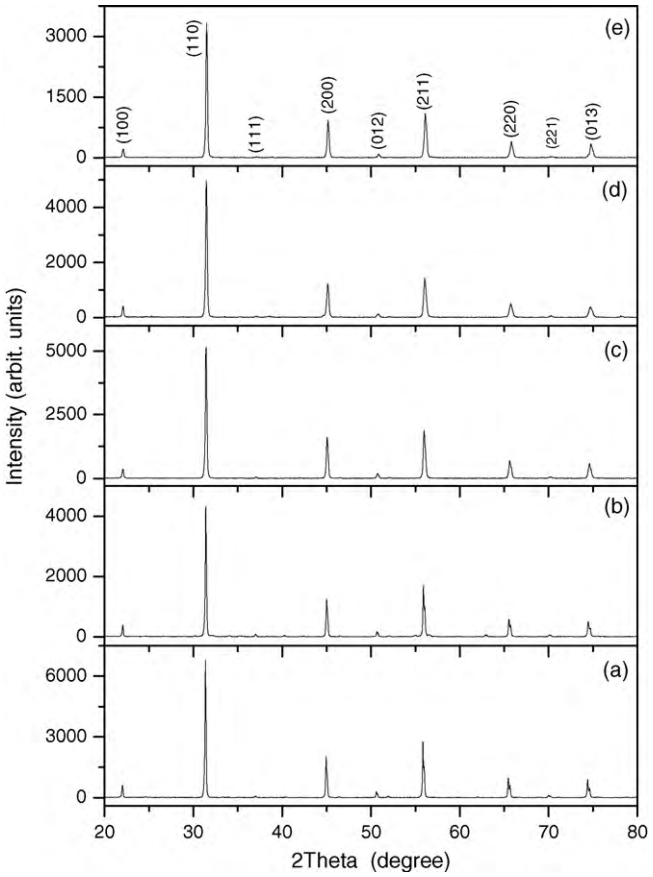

Fig. 1. XRD patterns of (a) $SrSnO_{3-\delta}$, (b) $SrSn_{0.95}Fe_{0.05}O_{3-\delta}$, (c) $SrSn_{0.9}Fe_{0.1}O_{3-\delta}$, (d) $SrSn_{0.85}Fe_{0.15}O_{3-\delta}$, and (e) $SrSn_{0.80}Fe_{0.2}O_{3-\delta}$.

except for the undoped $SrSnO_{3-\delta}$ and for $SrSn_{0.8}Fe_{0.2}O_{3-\delta}$. The activation energy E_a derived from the slopes of the graphs are 0.45, 0.41, 0.42 and 0.35 eV respectively for $SrSn_{0.95}Fe_{0.05}O_{3-\delta}$, $SrSn_{0.9}Fe_{0.1}O_{3-\delta}$, $SrSn_{0.85}Fe_{0.15}O_{3-\delta}$ and $SrSn_{0.8}Fe_{0.2}O_{3-\delta}$. E_a varies from 0.4 to 0.45 eV for $x = 0.05$, 0.1 and 0.15 compositions except for $x = 0.2$ for which the E_a is 0.35 eV [1,11]. Repeated measurements carried out on $x = 0.2$ gave the same E_a value. The activation energy of conduction for $SrSnO_{3-\delta}$ in the temperature range of 383–723 K is only 0.13 (±0.01) eV with an extremely poor conductivity of $1 \times 10^{-10}\ \Omega^{-1}\ cm^{-1}$ at 373 K. However, the Fe-doped $SrSn_{1-x}Fe_xO_{3-\delta}$ ($x = 0.05$–0.2) exhibit high electrical conductivity due to the charge carriers introduced by the substituent. To be used as a material for oxygen sensing, the given composition should exhibit significant change in electrical conductivity for a specific change in oxygen partial pressure at a given operating temperature of the sensor. Among the compositions investigated, electrical conductivity of $SrSn_{1-x}Fe_xO_{3-\delta}$ ($x = 0.1$ and 0.15) at different oxygen partial pressures is shown in Fig. 5. The other compositions exhibited only very marginal dependence of conductivity on oxygen partial pressures in the entire temperature range of investigation and therefore their plots are not shown. Although the change in conductivity of $SrSn_{0.85}Fe_{0.15}O_{3-\delta}$ is marginally lower than that of $SrSn_{0.9}Fe_{0.1}O_{3-\delta}$ for the specified change in oxygen partial pressures, the influence of moisture on conductivity of the system is relatively less as compared to that of the later. Thus, the preliminary investigations have shown that $SrSn_{0.85}Fe_{0.15}O_{3-\delta}$ is promising.

XPS patterns of $SrSn_{1-x}Fe_xO_{3-\delta}$ ($x = 0.05$–0.2) were recorded to investigate the chemical status of different elements in order to understand the mechanism of conductivity which is important for conductivity-based sensors. Table 1 summarizes the results obtained from the XPS analysis of the above samples. Fig. 6 shows

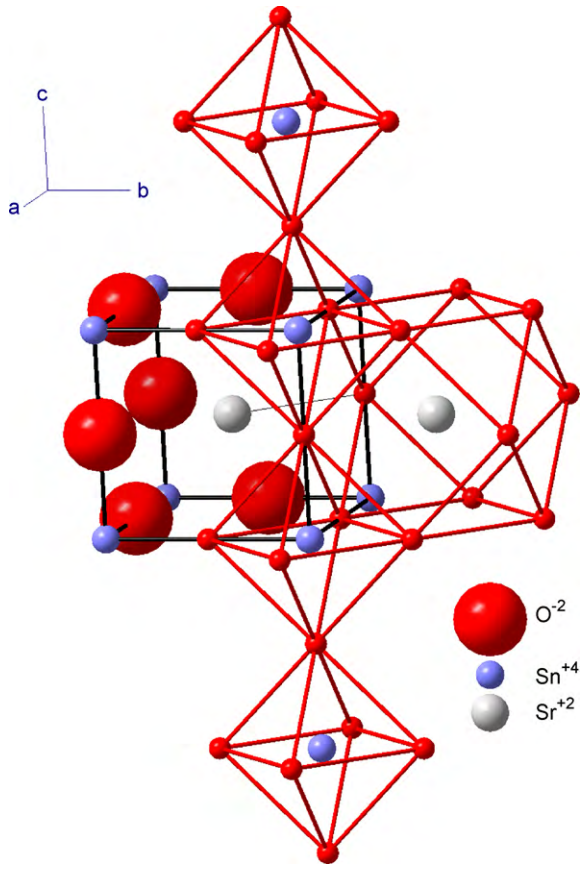

Fig. 2. Unit cell of $SrSnO_3$ perovskite structure showing the lattice sites of Sr- and Sn-ions.

the XPS spectra of Sr-3d level in $SrSn_{1-x}Fe_xO_{3-\delta}$ (x = 0.05–0.2) which exhibits a doublet pattern for $3d_{3/2}$ and $3d_{3/2}$ components. The background subtracted peaks were fitted with Gaussian functions giving rise to a correlation coefficient of 0.99. The peak position of the $3d_{5/2}$ and $3d_{3/2}$ components were at 133.6 and 135.6 eV respectively. Clearly, they are the finger prints of the divalent Sr-ions [12]. No other extra peak could be detected implying that all the Sr-ions are in divalent state. The peak positions of Sr-3d level do not change across the compositions even though Fe is increased from 0.05 to 0.2. This implies that Sr-ions are in divalent state in all the four compositions and that the partial substitution

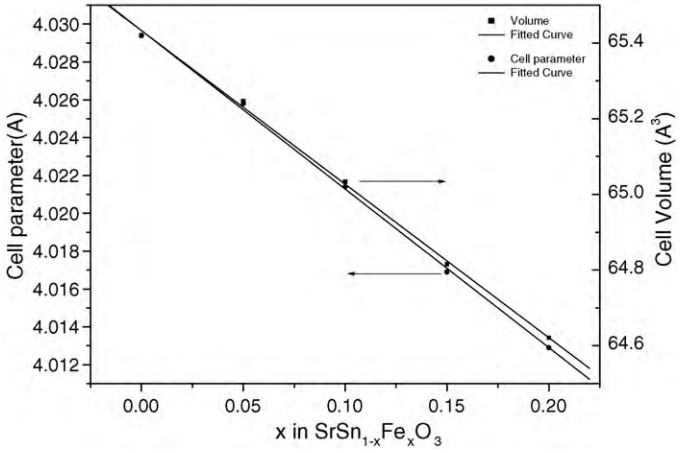

Fig. 3. Variation in unit cell volume as a function of Fe concentration in $SrSn_{1-x}Fe_xO_{3-\delta}$ (x = 0, 0.05, 0.1, 0.15 and 0.2).

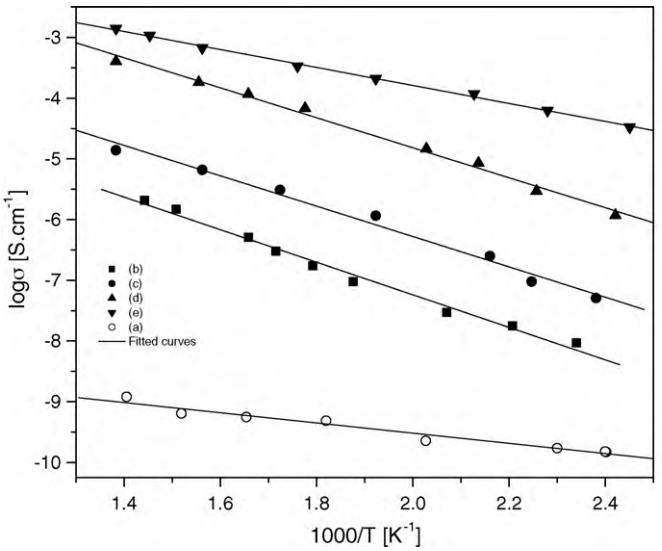

Fig. 4. Arrhenius plots for electrical conductivities of $SrSn_{1-x}Fe_xO_{3-\delta}$ (x = 0–0.2) in air.

of Fe does not influence its chemical status. Fig. 7 shows the XPS patterns of Sn-3d level for $SrSn_{1-x}Fe_xO_{3-\delta}$ (x = 0.05–0.2). The binding energies of the doublets $3d_{5/2}$ and $3d_{3/2}$ are observed at 486 and 493 eV respectively. The peaks were fitted with the combination of Gaussian–Lorentian curves which gave the correlation coefficient of 0.99. No other peaks could be detected implying that all the Sr-ions were in similar valence state across the compositions. Moreover, the peak positions indicate that all the Sn-ions are present in tetravalent state [12,13]. As both Sr-ions and Sn-ions

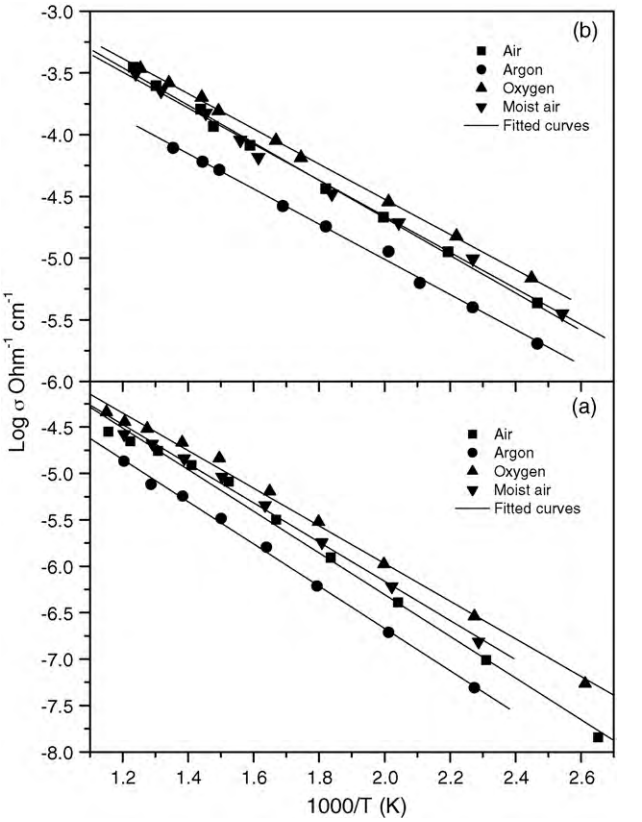

Fig. 5. Arrhenius plots of (a) $SrSn_{0.9}Fe_{0.1}O_{3-\delta}$ and (b) $SrSn_{0.85}Fe_{0.15}O_{3-\delta}$ in various ambient.

Table 1
The XPS parameters derived from the curve fit for Sr-3d, Sn-3d, Fe-2p and O-1s of $SrSn_{0.95}Fe_{0.05}O_{3-\delta}$.

S. No.	Composition	Energy level	Peak centre (eV)	FWHM (eV)	Area
1.	$SrSn_{0.95}Fe_{0.05}O_{3-\delta}$	Sr-$5d_{5/2}$	133.5 (±0.07)	1.55 (±0.04)	12175 (±129)
		Sr-$3d_{3/2}$	135.27 (±0.07)	1.58 (±0.04)	8240 (±56)
		O-1s	530.32 (±0.08)	1.72 (±0.07)	30471 (±213)
			532.25 (±0.08)	1.75 (±0.07)	5828 (±62)
		Sn-$3d_{5/2}$	486.78 (±0.05)	1.41 (±0.02)	62796 (±198)
		Sn-$3d_{3/2}$	495.16 (±0.05)	1.41 (±0.02)	43219 (±117)
2.	$SrSn_{0.90}Fe_{0.10}O_{3-\delta}$	Sr-$5d_{5/2}$	133.55 (±0.07)	1.5 (±0.04)	16951 (±134)
		Sr-$3d_{3/2}$	135.3 (±0.07)	1.43 (±0.04)	10954 (±66)
		O-1s	530.28 (±0.08)	1.66 (±0.07)	32494(±226)
			532.26(±0.08)	1.72 (±0.07)	5647 (±81)
		Sn-$3d_{5/2}$	486.72 (±0.05)	1.49 (±0.02)	55775 (±210)
		Sn-$3d_{3/2}$	495.14 (±0.05)	1.43 (±0.02)	37298 (±116)
3.	$SrSn_{0.85}Fe_{0.15}O_{3-\delta}$	Sr-$5d_{5/2}$	133.5 (±0.07)	1.58 (±0.04)	4842 (±143)
		Sr-$3d_{3/2}$	135.25 (±0.07)	1.58 (±0.04)	3325 (±76)
		O-1s	530.3 (±0.08)	1.73 (±0.07)	12164 (±322)
			532.1 (±0.08)	1.78 (±0.07)	2648 (±45)
		Sn-$3d_{5/2}$	486.5 (±0.05)	1.53 (±0.02)	30619 (±231)
		Sn-$3d_{3/2}$	494.9 (±0.05)	1.53 (±0.02)	20893 (±108)
4.	$SrSn_{0.80}Fe_{0.20}O_{3-\delta}$	Sr-$5d_{5/2}$	133.6 (±0.07)	1.45 (±0.04)	16618 (±124)
		Sr-$3d_{3/2}$	135.4 (±0.07)	1.45 (±0.04)	11235 (±120)
		O-1s	530.28 (±0.08)	1.54 (±0.07)	30082 (±237)
			532.09 (±0.08)	1.55 (±0.07)	5986 (±111)
		Sn-$3d_{5/2}$	486.77 (±0.05)	1.40 (±0.02)	59267 (±311)
		Sn-$3d_{3/2}$	495.2 (±0.05)	1.39 (±0.02)	40741 (±142)

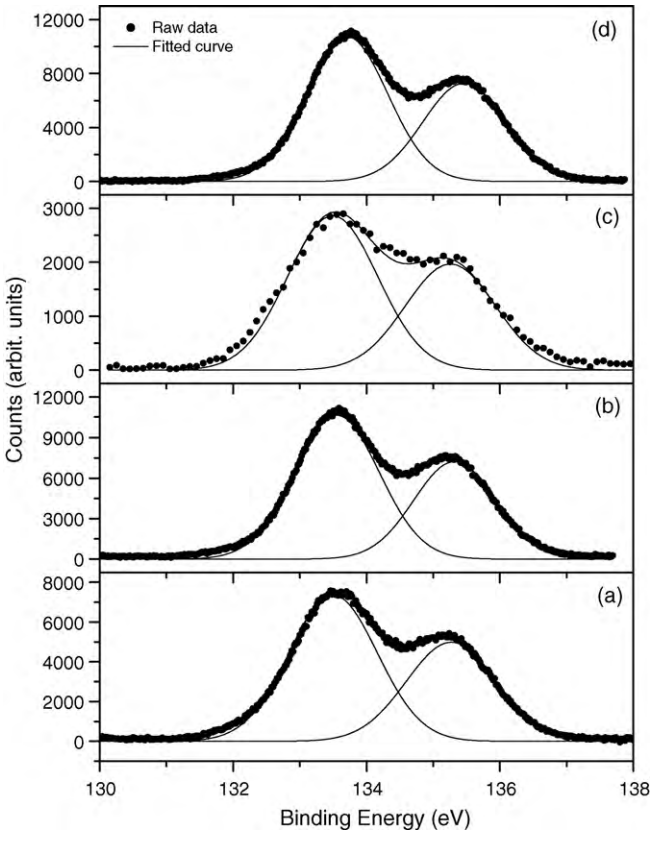

Fig. 6. XPS spectra of Sr-3d level with its $3d_{5/2}$ and $3d_{3/2}$ components in (a) $SrSn_{0.95}Fe_{0.05}O_{3-\delta}$, (b) $SrSn_{0.9}Fe_{0.1}O_{3-\delta}$, (c) $SrSn_{0.85}Fe_{0.15}O_{3-\delta}$, and (d) $SrSn_{0.80}Fe_{0.2}O_{3-\delta}$.

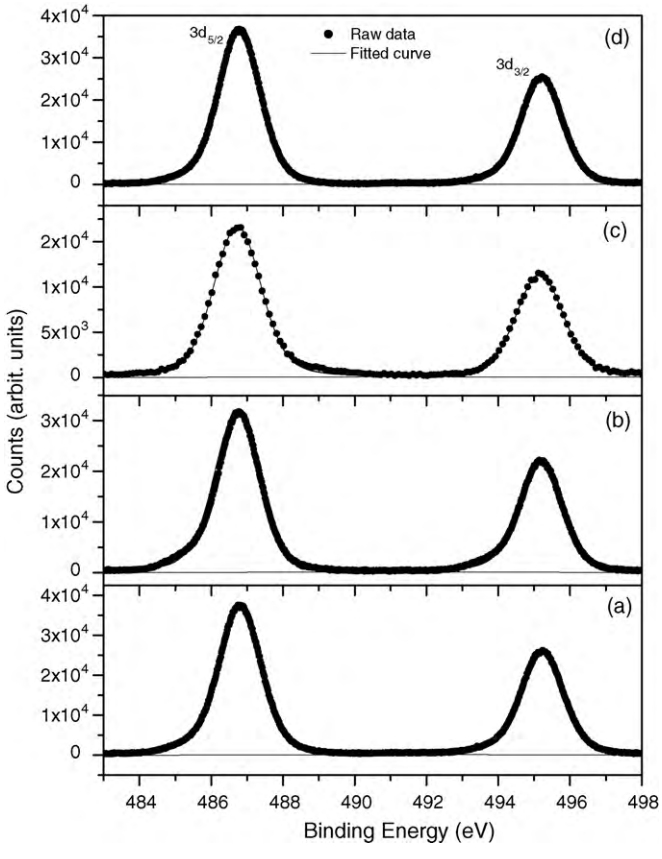

Fig. 7. XPS spectra of Sn-3d level with its $3d_{5/2}$ and $3d_{3/2}$ components in (a) $SrSn_{0.95}Fe_{0.05}O_{3-\delta}$, (b) $SrSn_{0.9}Fe_{0.1}O_{3-\delta}$, (c) $SrSn_{0.85}Fe_{0.15}O_{3-\delta}$, and (d) $SrSn_{0.80}Fe_{0.2}O_{3-\delta}$.

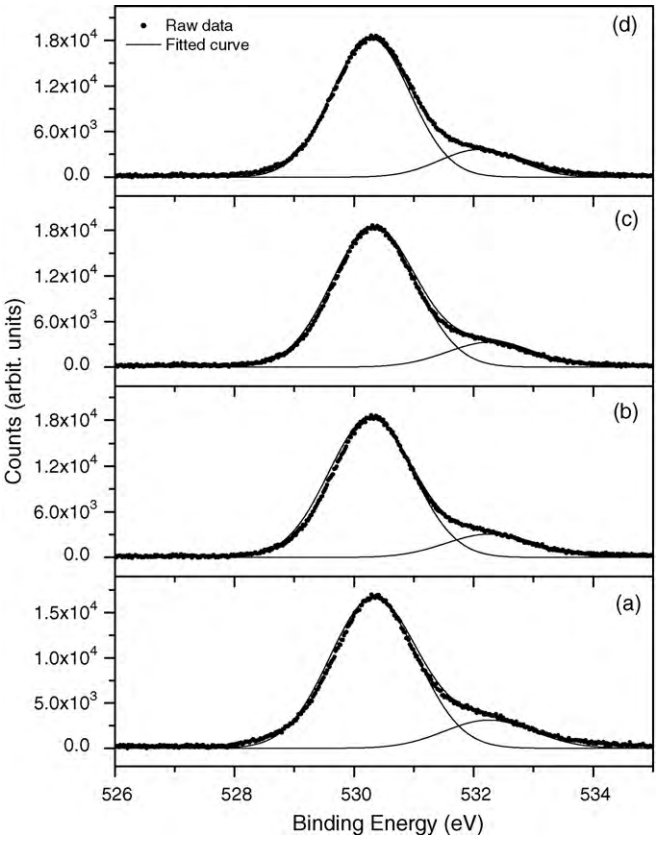

Fig. 8. XPS spectra of O-1s level in (a) $SrSn_{0.95}Fe_{0.05}O_{3-\delta}$, (b) $SrSn_{0.9}Fe_{0.1}O_{3-\delta}$, (c) $SrSn_{0.85}Fe_{0.15}O_{3-\delta}$, and (d) $SrSn_{0.80}Fe_{0.2}O_{3-\delta}$.

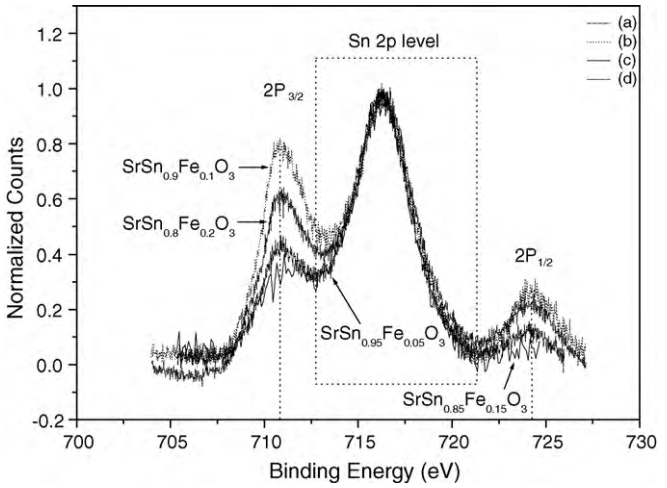

Fig. 9. XPS spectra of Fe-2p level with its $2p_{3/2}$ and $2p_{1/2}$ components in (a) $SrSn_{0.95}Fe_{0.05}O_{3-\delta}$, (b) $SrSn_{0.9}Fe_{0.1}O_{3-\delta}$, (c) $SrSn_{0.85}Fe_{0.15}O_{3-\delta}$, and (d) $SrSn_{0.80}Fe_{0.2}O_{3-\delta}$.

did not show any change in valence states across the compositions, chemical status of oxygen was probed. Fig. 8 shows the XPS pattern of O-1s level for $SrSn_{1-x}Fe_xO_{3-\delta}$ ($x = 0.05$–0.2). Deconvolution of the pattern gives rise to two different peaks which correspond to two different oxygen species. The major peak is observed at 530 eV whereas the minor peak is observed at 532.2 eV. The overall fit gives rise to a correlation coefficient of 0.99. The first peak observed at 530 eV is characteristic of O^{2-} lattice oxygen whereas the second minor peak observed at 532.2 eV could possibly be due to either of the following species viz., adsorbed moisture, hydroxyl groups or chemisorbed oxygen species [12,14]. Similar pattern is observed for other compositions also indicating the presence of adsorbed moisture or hydroxyl groups or chemisorbed oxygen in addition to the lattice oxygen. It is difficult to assign the binding energy of 532 eV to any particular species based on the available results.

As Sr-, Sn-ions and lattice-oxygen in $SrSnO_{3-\delta}$ remain in divalent state, tetravalent state and divalent state respectively even after doped with Fe, the sharp increase in conductivity with partial substitution of Fe is most likely due to Fe, the only remaining element known for its mixed valence characteristics in oxide systems. Hence, XPS patterns of Fe-2p levels were investigated. Fig. 9 shows the normalized, background corrected XPS patterns of Fe $2p_{3/2}$ and $2p_{1/2}$ in $SrSn_{1-x}Fe_xO_{3-\delta}$ ($x = 0.05$–0.2). Three peaks were observed as against the doublet pattern expected for $2p_{3/2}$ and $2p_{1/2}$ components. The peak positions are 710 and 719 eV respectively for $2p_{3/2}$ and $2p_{1/2}$ [15,16]. The third peak observed at 716 eV is highly intense and remains constant irrespective of the concentration of Fe indicating it might have a different origin. This third peak is due to Sn-$3p_{3/2}$ level and its component $3p_{1/2}$ is expected to occur at 756 eV which is not covered in the region of investigation. As the strong and intense peak of Sn $3p_{3/2}$ overlaps with the relatively less intense Fe $2p_{3/2}$ peak, deconvolution becomes complicated unless the former is safely removed without affecting the latter. Owing to the ensuing uncertainties involved, the oxidation states of Fe were not obtained from the XPS studies and Mossbauer studies were carried out on these samples to investigate the valence states of Fe.

Fig. 10 shows the Mossbauer spectra of Fe recorded for $SrSn_{1-x}Fe_xO_{3-\delta}$ ($x = 0.1$–0.2) samples at room temperature. Table 2 shows the isomer shift values of Fe-ions in different samples deduced from their spectra. Fe^{4+} has an isomer shift close to zero [17–19] whereas Fe^{+3} and Fe^{+2} have the values of ≤ 0.5 and $\leq 1\ mm\ s^{-1}$ respectively [20]. The uncertainty in peak fitting for all possible oxidation states of iron in these compositions is equally distributed. The overall pattern obtained from the deconvoluted components fits well with the experimentally observed spectra giving a statistical chi-square normalized value around 1.1 which indicates a reasonably good fit. The Mossbauer spectra of $SrSn_{0.8}Fe_{0.2}O_{3-\delta}$ is shown in Fig. 10(b) which clearly confirms that Fe is in three different oxidation state viz., Fe^{4+}, Fe^{3+} and Fe^{2+}. The results obtained with samples of other compositions were similar. For comparison, Mossbauer spectra of $SrFeO_{3-\delta}$ is also recorded and shown in Fig. 10(a). It shows two well-resolved peaks characteristic of only Fe^{4+} and Fe^{2+}. The relative amounts of different Fe species estimated from the area under the individual deconvoluted graphs corresponding to the respective oxidation state of Fe in each composition are also given in Table 2. It is to be pointed out that the Mossbauer results of Beurmann et al. and Roh et al. have indicated the presence of only Fe^{4+} and Fe^{3+} in these systems [9,11]. In $SrFeO_{3-\delta}$, the relative amounts of Fe^{4+} and Fe^{3+} are 78 and 22% respectively whereas in $SrSn_{0.8}Fe_{0.2}O_{3-\delta}$, Fe^{4+} decreases to 48% while and Fe^{3+} and Fe^{2+} are 15 and 38% respectively (Fig. 10(b)). The relative concentrations of Fe^{4+}, Fe^{3+}, Fe^{2+}, ions in $SrSn_{0.85}Fe_{0.15}O_{3-\delta}$ are 58, 12 and 30% respectively (Fig. 10(c)) and in $SrSn_{0.9}Fe_{0.1}O_{3-\delta}$, the corresponding amounts are 45.4, 19.7 and 34.9% respectively (Fig. 10(d)).

Although one may argue that there is no significant change in the relative concentration of the different species of Fe to account for the increase in conductivity across the compositions, the total amount of Fe^{3+} and Fe^{2+}, the species responsible for conductivity increases as one goes from Fe = 0.05 to 0.2. It should be pointed that the substitution of isovalent Fe^{4+} for Sn^{4+} does play a significant role in conductivity. The total percentage of Fe^{2+} and Fe^{3+} is 54.6, 42 and 52.4% respectively for $x = 0.1$, 0.15 and 0.2 [Table 2] (the total amount of lower valence Fe ions is arrived by $0.1 \times 0.054 = 0.054$ for $x = 0.1$, $0.15 \times 0.042 = 0.064$ for $x = 0.15$ and $0.2 \times 0.052 = 0.104$

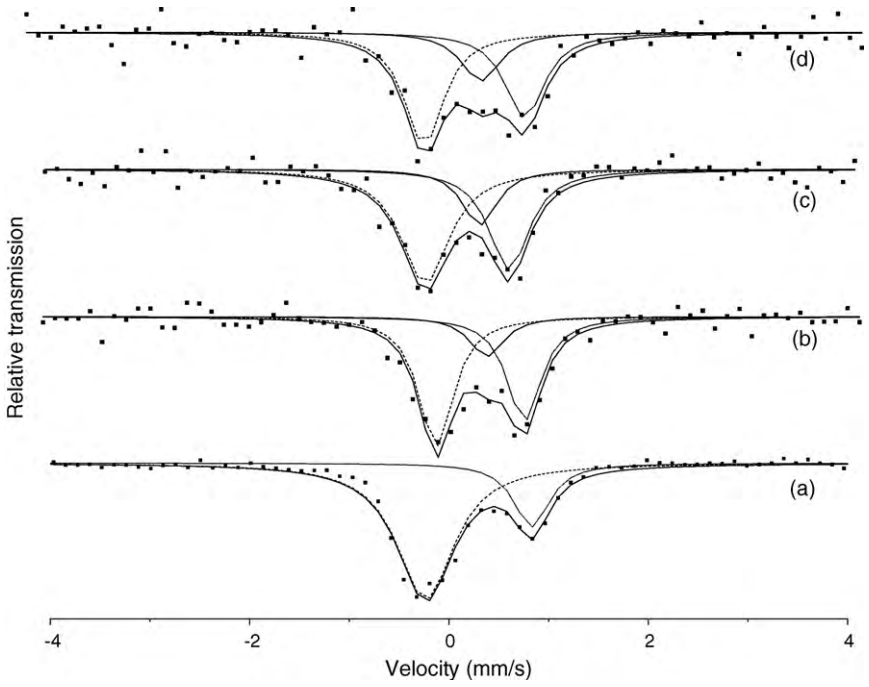

Fig. 10. Mossbauer studies for estimating different oxidation states of Fe in (a) $SrFeO_{3-\delta}$ [Fe^{+4} = 78% and Fe^{+2} = 22%], (b) $SrSn_{0.8}Fe_{0.2}O_{3-\delta}$ [Fe^{+4} = 48%, Fe^{+3} = 14% and Fe^{+2} = 38%], (c) $SrSn_{0.85}Fe_{0.15}O_{3-\delta}$ [Fe^{+4} = 58%, Fe^{+3} = 12% and Fe^{+2} = 30%], and (d) $SrSn_{0.9}Fe_{0.1}O_{3-\delta}$ [Fe^{+4} = 45%, Fe^{+3} = 20% and Fe^{+2} = 35%].

for $x = 0.2$). The overall increase in Fe proportionately increases the amount of Fe^{2+} and Fe^{3+} ions which in turn is responsible for the high conductivity with the increase in concentration of Fe. The mechanism of electrical conductivity and oxygen sensing can be explained as follows. Upon iron substitution in $SrSnO_3$, Fe enters into Sn^{+4} site and exist in three different oxidation states (+4, +3 and +2) as seen from Mossbauer studies. But, during this process, it generates electrons in the lattice as a consequence of oxide ion vacancies for electrical charge neutrality. Electrons are generated by oxygen loss from the lattice according to the following relation:

$$O_o \Leftrightarrow \tfrac{1}{2}O_2 + \ddot{V}_o + 2e^- \quad (1)$$

Nevertheless, it retains the p-type behaviour with holes as major charge carrier [1]. As Fe^{4+} do not produce a hole, only Fe^{3+} or Fe^{2+} in the lattice generated holes as explained below and introduce acceptor levels close to the valence band.

$$Fe_{Sn} \leftrightarrow Fe_{Sn}{}^{3+} + \dot{h} \quad (2)$$

$$Fe_{Sn} \leftrightarrow Fe_{Sn}{}^{2+} + 2\dot{h} \quad (3)$$

Thus, as a function of iron substitution, in $SrSn_{1-x}Fe_xO_{3-\delta}$ ($x = 0$, 0.05, 0.1, 0.15 and 0.2), a systematical increase in electrical conductivity is seen in the temperature range of 383–823 K in their respective Arrhenius plots (Fig. 4). However, at lower partial pressures of oxygen (below 21% O_2), more electrons are generated in the donor level in addition to the oxide ion vacancies reflecting in decrease of its electrical conductivity (Fig. 5(a) and (b)). This can be attributed to the annihilation of the holes present in the sample that is responsible for p-type conductivity. On the other hand, at higher partial pressures of oxygen (21–100% O_2), more holes are generated in the acceptor level as the non-stoichiometry in oxygen is considerably reduced. Thus, an increase in electrical conductivity is observed at higher oxygen partial pressures. This p-type behaviour is still clearly demonstrated by the strong oxygen partial pressure dependence conductivity and sensor studies between 15 and 50% of oxygen for the composition $SrSn_{0.85}Fe_{0.15}O_{3-\delta}$ at 773 K (Fig. 11(a) and (b)).

The oxide ion vacancy (oxygen non-stoichiometry) arising from Fe^{2+} and Fe^{3+} ions in $SrSn_{1-x}Fe_xO_{3-\delta}$ ($x = 0.05$–0.2) is under equilibrium with the oxygen partial pressure in accordance with Eq. (1) and if the oxygen partial pressure is varied, the equilibrium will shift accordingly affecting the overall vacancy concentration. In the

Table 2
Mossbauer parameters derived from the spectra of $SrFeO_{3-\delta}$, $SrSn_{0.8}Fe_{0.2}O_{3-\delta}$, $SrSn_{0.85}Fe_{0.15}O_{3-\delta}$ and $SrSn_{0.9}Fe_{0.1}O_{3-\delta}$ with respect to iron (α-bcc) at 301 K.

[Mossbauer spectroscopy analyzed data with respect to iron (α-bcc) at 301 K]					
Sample	Isomer shift (mm/s)	Quadrupole shift (mm/s)	FWHM (mm/s)	Area %	Species
$SrFeO_{3-\delta}$	−0.12	0.09	0.68	77.6	Fe^{4+}
	0.94	0.08	0.41	22.4	Fe^{2+}
$SrSn_{0.80}Fe_{0.20}O_{3-\delta}$	−0.10	0.09	0.45	47.6	Fe^{4+}
	0.41	0.08	0.45	14.6	Fe^{3+}
	0.79	0.08	0.45	37.8	Fe^{2+}
$SrSn_{0.85}Fe_{0.15}O_{3-\delta}$	−0.14	0.09	0.57	58	Fe^{4+}
	0.41	0.08	0.45	12.2	Fe^{3+}
	0.70	0.08	0.47	29.8	Fe^{2+}
$SrSn_{0.90}Fe_{0.10}O_{3-\delta}$	−0.15	0.09	0.45	45.4	Fe^{4+}
	0.41	0.08	0.45	19.7	Fe^{3+}
	0.84	0.08	0.45	34.9	Fe^{2+}

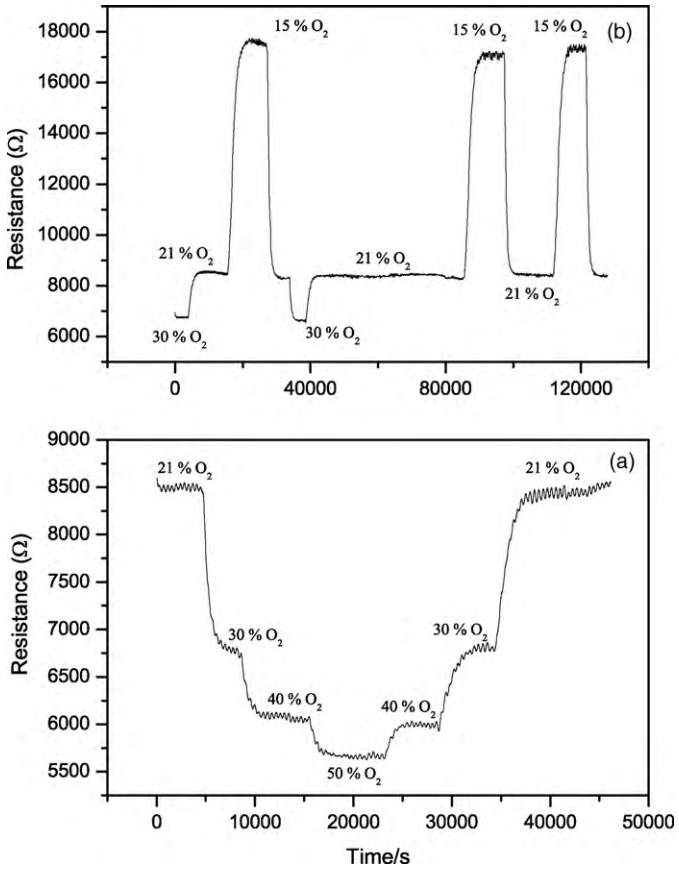

Fig. 11. Sensor study of $SrSn_{0.85}Fe_{0.15}O_{3-\delta}$ bulk pellet at 773 K for (a) 21–50% O_2 and (b) 30–15% O_2.

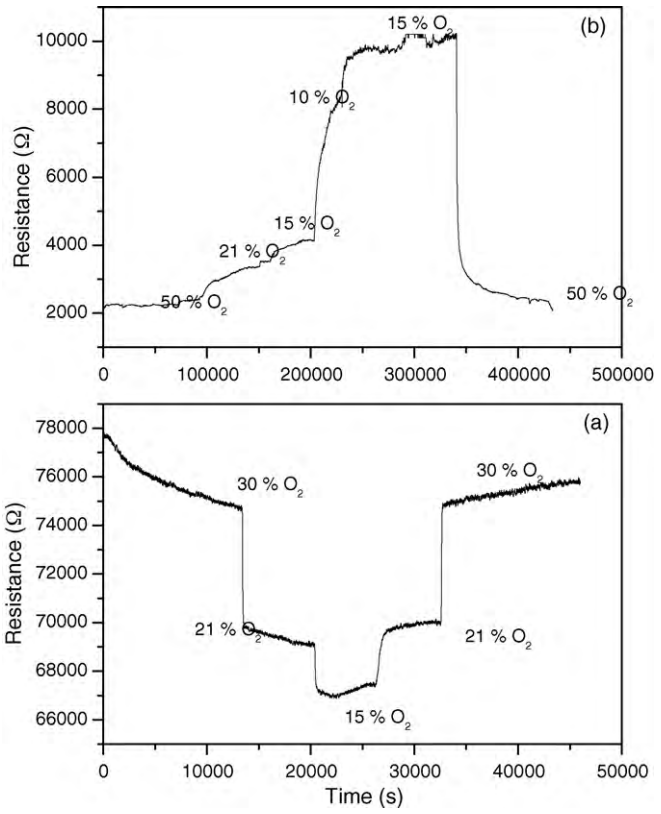

Fig. 12. Response characteristics of bulk pellets of (a) $SrSn_{0.85}Fe_{0.10}O_{3-\delta}$ and (b) $SrSn_{0.85}Fe_{0.10}O_{3-\delta}$ at 773 K.

case of n-type semiconductor oxides, the conduction electrons are usually trapped by the oxygen ions adsorbed on the surface due to its high electro-negativity. The change in equilibrium concentration of the adsorbed species introduces corresponding changes in electrical conductivity which is the accepted mechanism of sensing. In contrast, the positively charged hole carriers of the p-type oxides cannot be trapped by the adsorbed oxygen and therefore, the direct participation of the adsorbed gas species in trapping the hole carriers is not proposed. However, as the hole carrier density depends sensitively on the oxide vacancies, the changes in equilibrium concentration of vacancies affect the electrical conductivity. It is quite likely that the adsorbed–desorbed oxygen species play a role in altering the vacancy concentration.

The primary condition for the material to be used as an oxygen sensor is that the material should exhibit a significant change in conductivity for the given partial pressure range of oxygen at a chosen temperature. The objective of this work is to find out the highly sensitive composition within the family of $SrSn_{1-x}Fe_xO_{3-\delta}$ which exhibits large changes in conductivity in the oxygen partial pressure of 10–20%. As seen earlier, the electrical conductivity of $SrSn_{0.85}Fe_{0.15}O_{3-\delta}$ changes significantly as a function of oxygen partial pressure with little interference from moisture. Therefore, detailed sensor studies were carried on this composition. Fig. 11(a) shows the transient changes in resistance of $SrSn_{0.85}Fe_{0.15}O_{3-\delta}$ bulk pellet at 773 K for 15, 21 and 30% O_2. It has a stable baseline value of 8.5 kΩ at 21% O_2 with a reasonable response of about 52% and recovery time of about 30 to 40 min. Reducing the oxygen partial pressure to 15% increases the resistance to 17.6 kΩ and increasing the oxygen partial pressure 30% decreases the resistance to 6.7 kΩ. For comparison, the response characteristics of $SrSn_{0.9}Fe_{0.1}O_{3-\delta}$ and $SrSn_{0.8}Fe_{0.2}O_{3-\delta}$ (Fig. 12(a) and (b)). At temperatures below 450 °C, all the compositions exhibited a poor response with long recovery times. The response and recovery times started improving with temperature and the former reached a maximum around 500 °C. Beyond 500 °C, the response came down although recovery times are reduced. Thus an operating temperature of 500 °C is chosen. The response pattern of $SrSn_{0.9}Fe_{0.1}O_{3-\delta}$ (Fig. 12(a)) towards different partial pressures of oxygen is relatively sharper as compared to that of $SrSn_{0.8}Fe_{0.2}O_{3-\delta}$ (Fig. 12(b)). But compared to that of $SrSn_{0.85}Fe_{0.15}O_{3-\delta}$, the response of the $SrSn_{0.9}Fe_{0.1}O_{3-\delta}$ is relatively inferior. Moreover, it suffers from the moisture interference as seen from the conductivity studies. Therefore, $SrSn_{0.85}Fe_{0.15}O_{3-\delta}$ was identified as the promising composition.

Generally, n-type semiconducting oxides exhibit decrease in resistance (increase in conductivity) due to oxygen non-stoichiometry which introduces donor levels [21]. At lower oxygen partial pressures, the deviation in oxygen non-stoichiometry will be even higher and therefore, there is a decrease in resistance further. The opposite trend observed for $SrSn_{1-x}Fe_xO_{3-\delta}$ ($x = 0.1$ and 0.15) as function of oxygen partial pressure shows that these composition exhibit a p-type behaviour. Repeated response pattern confirms the reproducibility of the sensor. However, the response and recovery times are quite long. This is due to three different factors namely, the large volume of the vessel (~150 cc) in which the tests were carried out, high porosity (33%) of the pellet and low flow rate (20 ml/min) of the gas used for test studies. Fig. 11(b) shows the transient change in resistance when the oxygen partial pressure is gradually decreased from 15% → 21% → 30% → 40% → 50% → 40% → 30% → 21% → 15%. The baseline resistance corresponding to each oxygen partial pressure is restored. Generally sensors made of bulk porous pellets

are not desirable as they take long time to respond and recover. Besides, these bulky devices are also not energy efficient. Even if high temperature is used to drive the kinetics of the diffusion-controlled reactions, the sensitivity (the change in conductivity for a specific change in partial pressure) became poor at higher temperatures. However, thin film structures (thickness ~ 1000 å) offer the scope to reduce the diffusion-controlled processes with considerable reduction in response and recovery times. Nanostructured thin films (sensor grade) with high-specific surface area are ideally suitable as gas sensors and therefore, fabrication of high quality nanostructured thin films of the most promising composition using pulsed laser deposition technique is the ultimate objective of this work.

4. Conclusions

$SrSn_{1-x}Fe_xO_{3-\delta}$ ($x = 0$–0.2) is stabilized in cubic phase (P23). The lattice parameter decreases linearly with Fe concentration. Electrical conductivity $SrSn_{1-x}Fe_xO_{3-\delta}$ ($x = 0$–0.2) increases with Fe concentration. The activation energy values of $SrSn_{1-x}Fe_xO_{3-\delta}$ ($x = 0$ to 0.2) are about 0.45 eV for all the compositions implying that the mechanism of electrical conduction is same. The chemical status of Sr, Sn and oxygen as investigated by XPS shows that they are in +2, +4 and −2 valence states respectively. XPS of Fe 2p could not be resolved because of the overlap of a strong Sn 3p peak. Mossbauer studies give the finger prints of +4, +3 and +2 valence states for iron and that the relative amount of these species remain same across $SrSn_{1-x}Fe_xO_{3-\delta}$ ($x = 0.5$–0.2). As Sr, Sn and oxygen are respectively in +2, +4 and −2 valence states, the observed change is conductivity of $SrSn_{1-x}Fe_xO_{3-\delta}$ ($x = 0.5$–0.2) is suggested to be due to Fe^{3+} and Fe^{2+} ions. A strong oxygen partial pressure dependence on conductivity is observed for $SrSn_{0.85}Fe_{0.15}O_{3-\delta}$ and the same is explored for gas sensor studies. This composition gives a p-type response to the variation in oxygen partial pressures from 15 to 30%. This composition can be used as conductivity based sensor material to measure percentage levels of oxygen at operating temperatures above 623 K.

Acknowledgements

Authors are thankful to the X-ray characterizing group in Chemistry Group, Mr. R. Asuvathraman for his help in drawing crystal structure for the compound, Ms. Ranita Paul, Mr. Pinaki Paul and Dr. R.K. Dayal, CSTD, MMG for helping to record spectra for the samples by XPS, Mr. P. Chandramohan and M.P. Srinivasan of WSCD, BARC (F) for recording Mossbauer spectra of the samples and finally Dr. P.R. Vasudeva Rao, Director, CG for his constant encouragement towards this work.

References

[1] V. Thangadurai, P. Schmid Beurmann, W. Weppner, Mater. Sci. Eng. B 100 (2003) 18.
[2] C.G. Fan, Z.Q. Deng, Y.B. Zuo, W. Liu, C.S. Chen, Solid State Ionics 166 (2004) 339.
[3] W.F. Zhang, J. Tang, J. Ye, Chem. Phys. Lett. 418 (2006) 174.
[4] I.R. Shein, V.L. Kozhevnikov, A.L. Ivanovskii, Solid State Sci. 10 (2008) 217.
[5] V. Thangadurai, P. Schmid Beurmann, W. Weppner, Mater. Res. Bull. 37 (2002) 599.
[6] V. Thangadurai, R.A. Huggins, W. Weppner, J. Power Sources 108 (2002) 64.
[7] Z.L. Wang, Z.C. Kang, Functional and Smart Materials: Structural Evolution and Structure Analysis, New York, 1998, p. 93.
[8] Y. Xu, X. Zhou, O.T. Sorensen, Sens. Actuators B 65 (2000) 2.
[9] P Schmid Beurmann, V. Thangadurai, W. Weppner, J. Solid State Chem. 174 (2003) 392.
[10] R.D. Shannon, Acta Crystallogr. A 32 (1976) 751.
[11] K.S. Roh, K.H. Ryu, C.H. Yo, J. Solid State Chem. 142 (1999) 288.
[12] N. Sharma, K.M. Shaju, G.V. Subba Rao, B.V.R. Chowdari, J Power Sources 139 (2005) 250.
[13] M.G. Kim, H.S. Cho, C.H. Yo, J. Phys. Chem. Sol. 59 (9) (1998) 1369.
[14] J.A. Leiro, M.H. Heinonen, K. Elboussiri, Phys. Rev. B 52 (1995) 82.
[15] T. Yamashita, P. Hayes, Appl. Surf. Sci. 254 (2008) 2441.
[16] A.P. Grosvenor, B.A. Kobe, M.C. Biesinger, N.S. McIntyre, Surf. Inter. Anal. 36 (2004) 1564.
[17] Y. Takeda, K. Kanno, T. Takeda, O. Yamamoto, M. Takano, N. Nakayama, Y. Bando, J. Solid State Chem. 63 (1986) 237.
[18] M. Takano, T. Okita, N. Nakayama, Y. Bando, Y. Takeda, O. Yamamoto, J.B. Goodenough, J. Solid State Chem. 73 (1988) 140.
[19] N.N. Greenwood, T.C. Gibb, Mossbauer Spectroscopy, Chapman and Hall Publications, London, 1971, p. 280.
[20] J. Silver, Chemistry of Iron, Chapman and Hall Publications, London, 1993, p. 177.
[21] V. Thangadurai, W. Weppner, Electrochim. Acta 50 (2005) 1871.